CVCF Control of a Matrix Converter-Based Single-Phase Three-Wire Isolated AC-DC Converter under Standalone Operation with Unbalanced Loads

Ryoki Onodera[1]*, Hiroki Watanabe[1], Jun-ichi Itoh[2], Naoto Izumoto[3], Takahiro Ohori[3]
1 Department of Electrical, Electronics and Information Engineering, Nagaoka University of Technology, Niigata, Japan
2 Department of Science of Technology Innovation, Nagaoka University of Technology, Niigata, Japan.
3 Advanced Technologies Innovation Center, Engineering Division, Panasonic Electric Works Co., Ltd., Osaka, Japan.
*s233112+onodera@stn.nagaokaut.ac.jp

***Abstract*— This paper proposes a CVCF control method for a matrix-converter-based single-stage isolated AC-DC converter under standalone operation of a single-phase three-wire system with unbalanced loads. The proposed method consists of a line-to-line voltage control loop and an imbalance compensation loop for suppressing neutral-point potential fluctuation. In the proposed converter, the high-frequency AC-link inductor current must also be regulated within each switching period. Therefore, the control variables δ and α are determined from the u-w phase current command and the neutral-line current command based on an inductor-current waveform model. In addition, the switching pattern is selected according to the polarity relationship between the line-to-line voltage and the neutral-line current. As a result, stable CVCF operation is maintained even when the heavier-load phase changes. Simulation results verify the effectiveness of the proposed method under steady-state unbalanced-load conditions, transitions between balanced and unbalanced loads, and load-step conditions.**

Keywords*— Dual active bridge converter, Standalone operation, Matrix converter, Single-phase three-wire

I. INTRODUCTION

In recent years, the installation of photovoltaic (PV) systems in residential applications has increased in order to promote decarbonization and improve energy resilience. In Japan, single-phase three-wire distribution lines are widely used in residential distribution systems. This distribution system allows 100 V_{RMS} loads to be connected to the neutral line while providing 200 V_{RMS} line-to-line voltage. The Power Conditioning System (PCS) requires both grid-connected and standalone operation in order to use PV-generated power effectively [1]. In grid-connected operation, the PCS transfers the generated power from PV to the single-phase grid. On the other hand, the PV-PCS operates as a distributed power source in standalone mode during emergency conditions [2-5].

CVCF control methods for conventional single-phase three-wire inverters have been reported in order to maintain output voltages under unbalanced or nonlinear load conditions [6]. Previous studies have shown that CVCF operation is maintained under such conditions by controlling the output voltages with PI controllers. On the other hand, residential PCSs require higher efficiency and higher power density. A typical isolated PCS uses a two-stage configuration consisting of an isolated DC-DC converter and a single-phase inverter [7]. However, this configuration requires multiple power-conversion stages, which increase conversion loss. In addition, the two-stage configuration requires a DC-link capacitor, which may increase the system size. Therefore, this configuration makes it difficult to achieve both high efficiency and high power density. For this reason, previous studies have investigated single-stage isolated converters, which eliminate the need for a DC-link capacitor in the two-stage configuration and reduce the number of power-conversion stages. Accordingly, a single-stage isolated AC-DC converter based on a single-phase matrix converter has been proposed [8-11]. This converter uses a high-frequency inverter to generate high-frequency AC, and a matrix converter on the transformer secondary side directly converts it to utility-frequency AC. This configuration uses no DC-link capacitor and reduces the number of power-conversion stages. Therefore, it improves efficiency.

However, when this single-stage isolated AC-DC converter is applied to a single-phase three-wire PCS and operated in standalone mode, the neutral-point potential fluctuation caused by load imbalance must be suppressed in order to maintain CVCF operation. When the neutral-point potential fluctuates, an amplitude difference appears between the output voltages of the u-o phase and the w-o phase, making it difficult to maintain each phase voltage as a 100 V_{RMS} sinusoidal waveform. In addition, unlike conventional voltage-source inverters, the proposed converter must treat the high-frequency AC-link inductor current as an additional control variable within each switching period. Therefore, the conventional CVCF scheme for voltage-source inverters cannot be directly applied to the proposed converter. The authors have previously investigated an imbalance compensation control method assuming prior knowledge of the load information. In this method, stable voltage control cannot be maintained when the heavier-load phase changes because the control strategy also changes according to the load condition.

This paper proposes a control method for maintaining CVCF operation in a single-phase three-wire single-stage isolated AC-DC converter based on a single-phase matrix converter, regardless of which phase carries the heavier load during standalone operation. The proposed control consists of two control loops: a voltage control loop for regulating the output line-to-line voltage to 200 V_{RMS} and an imbalance compensation control loop for suppressing the neutral-point potential fluctuation. In addition, the control variables δ and α

are determined from the u-w phase current command and the neutral-line current command based on an inductor-current waveform model. Furthermore, the switching pattern is selected according to the polarity relationship between the line-to-line voltage and the neutral-line current. The main feature of the proposed method is that the output voltage of each phase is stably maintained without changing the control configuration, even when the heavier-load phase changes. Simulation results confirm that CVCF operation is maintained even under unbalanced load conditions with phase-to-phase load variations.

II. CIRCUIT CONFIGURATION

A. Conventional Circuit

Fig. 1 shows the conventional isolated DC-AC converter. The conventional circuit consists of an isolated DC-DC converter and a single-phase three-wire inverter and has a two-stage configuration with a DC link. Several topologies, such as full-bridge converters, serve as the isolated DC–DC stage. This paper adopts a Dual Active Bridge (DAB) converter as the conventional configuration and assumes bidirectional power control. As shown in Fig. 1, this circuit requires two-stage power conversion. Therefore, the conversion loss increases and the efficiency decreases.

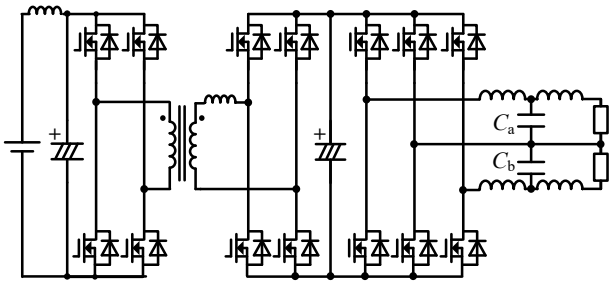

Fig. 1. Isolated two-stage AC–DC conventional converter for single-phase three-wire.

B. Proposed Circuit

Fig. 2 shows the proposed circuit. The proposed circuit connects a single-phase matrix converter to the transformer secondary, forming a single-stage configuration without a DC link. The control principle is the same as that of the DAB converter, and bidirectional power control is achieved by phase-shift control. The conventional circuit achieves CVCF operation by regulating the terminal voltages of the AC side filter capacitors C_a and C_b. In contrast, the proposed controller must treat the high-frequency AC-link inductor current as an additional control variable within each switching period. Therefore, the conventional CVCF scheme for voltage-source inverters cannot be directly applied to the proposed circuit.

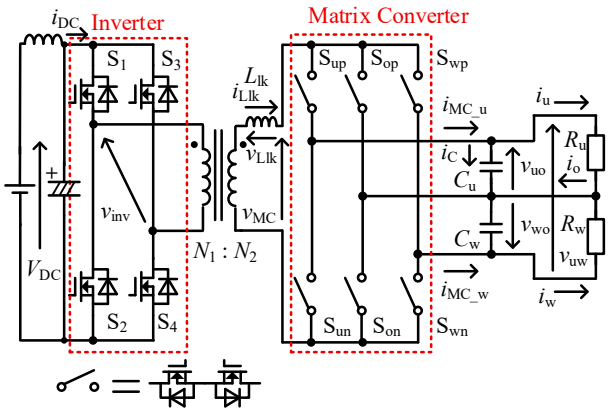

Fig. 2. Isolated single-stage AC–DC converter with a matrix converter for single-phase three-wire.

Accordingly, this paper investigates a CVCF control method for the proposed circuit shown in Fig. 2. The proposed control introduces a voltage control loop to regulate the output line-to-line voltage v_{uw} and an additional control loop to compensate for neutral-point potential imbalance.

III. CONTROL METHOD

A. CVCF Control Method

Fig. 3 shows the switching pattern of the matrix converter and the high-frequency inverter. Fig. 3 shows the switching pattern for the case where the w-phase output power is smaller than the u-phase output power ($P_w < P_u$). The switching period is denoted by T_{sw}, and each operating interval is determined accordingly. The high-frequency inverter operates with a duty ratio of 0.5, and the matrix converter applies voltages to the u-o and u-w phases. The phase shift δ represents the delay of the matrix converter output voltage v_{MC} with respect to the rising edge of the high-frequency inverter output voltage v_{inv}. The parameter α represents the interval during which the proposed method applies voltage to the u–w phase. This interval corresponds to the duration in which either the upper switches or the lower switches in the u-phase leg and the w-phase leg of the matrix converter turn on simultaneously. In the control based on the switching pattern shown in Fig. 3, δ is the primary control variable for adjusting the output voltage and

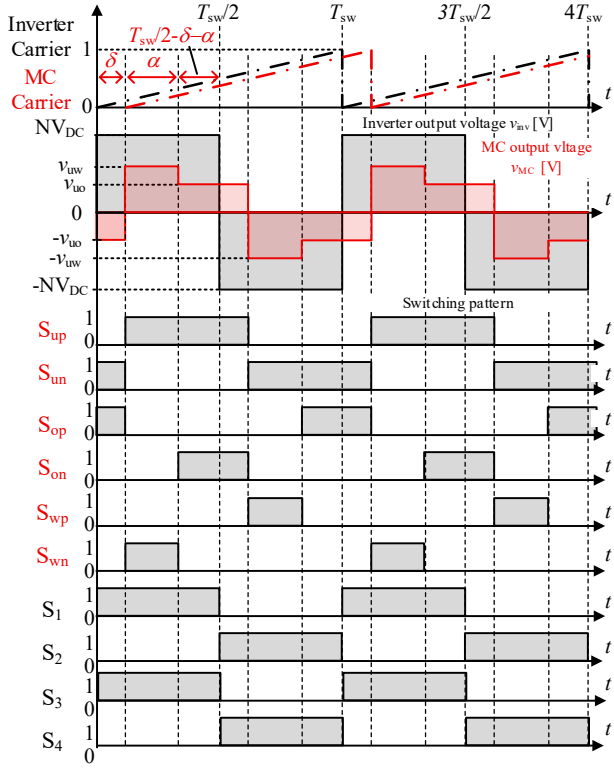

Fig. 3. Gate pulse waveform of the proposed method.

the load power. In addition, controlling α and the u-o phase voltage application interval, which corresponds to $T_{sw}/2 - \delta - \alpha$ in Fig. 3, adjusts the average value of each phase current.

Under an unbalanced load in a single-phase three-wire system, active power sharing among phases becomes non-uniform and the neutral-point potential varies. As a result, the u–o and w–o output voltages, which ideally have equal

amplitude and a 180 degrees phase difference, become asymmetric and show an amplitude difference. This paper compensates for neutral-point potential fluctuation by controlling δ and α so as to adjust the phase currents. Consequently, the proposed control achieves CVCF operation in the single-phase three-wire system even under unbalanced load conditions.

When the w-phase output power exceeds the u-phase output power ($P_u < P_w$), the voltage applied to the transformer in Fig. 3 changes from v_{uo} to v_{wo}. In this case, exchanging the switching functions S_{ux} and S_{wx} of the u-phase leg and the w-phase leg yields the switching pattern of the matrix converter. The subscript x denotes both the P-arm and the N-arm. The relationship between the heavier-load phase and the neutral-line current i_o determines the switching pattern.

Fig. 4 shows the waveforms of the u-w line-to-line voltage v_{uw}, the u-phase output current i_u, the w-phase output current i_w, and the neutral-line current i_o under balanced and unbalanced load conditions. Under balanced-load conditions ($P_u = P_w$), i_u and i_w have the same amplitude, and i_o is zero. When $P_u > P_w$, i_u has a larger amplitude than i_w, and i_o is in phase with v_{uw}. Conversely, when $P_u < P_w$, i_w has a larger amplitude than i_u, and i_o is out of phase with v_{uw}.

The heavier-load phase can therefore be identified from the polarity relationship between v_{uw} and i_o. Specifically, the u-phase is the heavier-load phase when v_{uw} and i_o have the same polarity, whereas the w-phase is the heavier-load phase when their polarities are opposite. Based on this relationship, the proposed control method maintains CVCF operation through switching pattern selection according to the sign relationship between v_{uw} and i_o.

B. Line-to-Line Voltage and Imbalance Compensation Control

Fig. 5 shows the control block diagram of the proposed CVCF control method. The output voltages of the single-phase three-wire system are the u-o phase voltage v_{uo} and the w-o phase voltage v_{wo}. These voltages must have the same amplitude and be 180 degrees out of phase. By controlling v_{uo} and v_{wo} to satisfy these conditions, the control method generates a 200 V_{RMS} sinusoidal line-to-line voltage v_{uw}.

Under unbalanced load conditions, fluctuations in the neutral-point potential cause an amplitude difference between v_{uo} and v_{wo}. To address this issue, this paper decomposes the single-phase three-wire output voltages into the differential-mode voltage v_{uw} and the common-mode voltage v_{cm}, and controls them independently. The voltages v_{uw} and v_{cm} are defined by (1) and (2), respectively.

$$v_{uw} = v_{uo} - v_{wo} \tag{1}$$

$$v_{cm} = \frac{v_{uo} + v_{wo}}{2} \tag{2}$$

The voltage v_{cm} corresponds to the neutral-point offset voltage that appears in the u-o and w-o phase voltages. The proposed control consists of a voltage control loop for regulating the line-to-line voltage v_{uw} and an imbalance compensation control loop for controlling the common-mode voltage v_{cm} to zero. By forcing v_{uw} to track its instantaneous reference, the controller maintains the desired line-to-line voltage. In addition, by controlling v_{cm} to zero, the neutral-point potential fluctuation caused by unbalanced loads is compensated. As a result, the proposed CVCF control

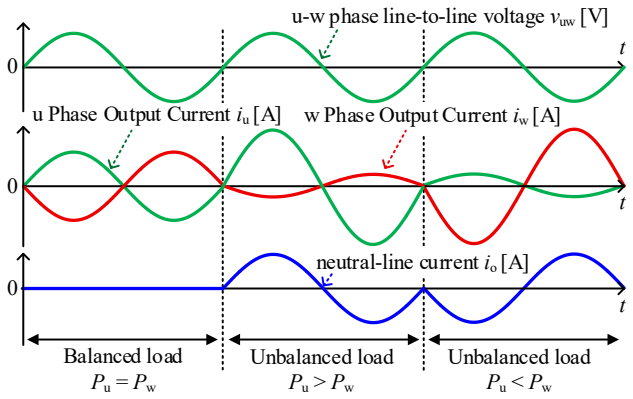

Fig. 4. Output Waveforms and Neutral-Line Current under Balanced and Unbalanced Load Conditions.

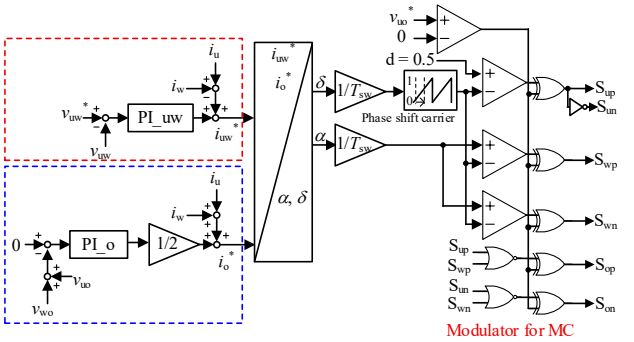

Fig. 5. Control block diagram of the proposed method.

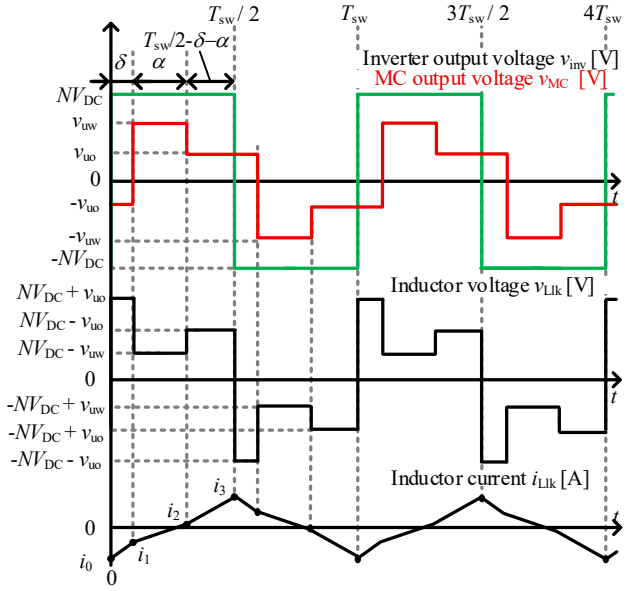

Fig. 6. Typical waveform of the proposed converter.

suppresses interphase voltage imbalance and maintains single-phase three-wire operation even under unbalanced load conditions.

In the proposed circuit, δ and α must also regulate the high-frequency-link inductor current within each switching period. The PI controllers generate the neutral-line current command i_o^* and the u-w phase current command i_{uw}^*. A δ-α calculation block placed after the PI controllers converts these current commands into the time intervals δ and α within the switching period. Based on the previously derived current–phase-shift and current–applied-time characteristics, this block determines the final values of δ and α from i_o^* and i_{uw}^*. In this study, the δ - α calculation block implements the parameter-determination procedure derived in Section III-C,

i.e., it computes (δ, α) from (i_o^*, i_{uw}^*) under the physical constraints in (12).

C. Characteristics of Current versus Phase Shift and Applied Time

Fig. 6 shows the waveforms of the matrix-converter output voltage v_{MC}, the high-frequency-inverter output voltage v_{inv}, and the inductor current i_{Llk} flowing through the leakage inductance L_{lk}. This section focuses on the case where the w-phase output power is smaller than the u-phase output power ($P_u > P_w$). In the opposite case ($P_u < P_w$), the circuit outputs -v_{uo} during the δ interval and v_{uo} during the T_{sw} / 2 - δ - α interval. Due to the symmetry of the circuit and the single-phase three-wire output with respect to the u and w phases, the subsequent derivations can also be applied to the case ($P_u < P_w$), provided that v_{uo} and v_{wo}, as well as i_u and i_w, are exchanged appropriately, together with the corresponding polarity of i_o and the switching pattern selected in Section III-A.

The slope of the inductor current i_{Llk} varies with the voltage applied across the leakage inductance L_{lk}. The following analysis therefore divides the operation into the δ interval, the α interval, and the remaining interval T_{sw} / 2 - δ - α, according to the relationship between v_{MC} and v_{inv}. Here, N denotes the turns ratio of the high-frequency transformer, and NV_{dc} denotes the dc voltage referred to the primary side. The current waveform is symmetric, and its sign changes every T_{sw} / 2. Therefore, the following discussion focuses only on the positive half-cycle. Integrating the current slope over each interval based on the voltage waveforms shown in Fig. 6 gives the current values in each mode within a half switching period. Here, i_0 denotes the current at the beginning of the half cycle, whereas i_1, i_2, and i_3 denote the currents at the mode transition instants. Equation (3) gives these currents.

$$\begin{cases} i_0 = -\dfrac{1}{2L_{leak}}\left\{(NV_{DC}+v_{uo})\delta + (NV_{DC}-v_{uw})\alpha + (NV_{DC}-v_{uo})\left(\dfrac{T_{sw}}{2}-\delta-\alpha\right)\right\} \\ i_1 = \dfrac{NV_{DC}+v_{uo}}{L_{leak}}\delta + i_0 \\ i_2 = \dfrac{NV_{DC}-v_{uw}}{L_{leak}}\alpha + i_1 \\ i_3 = \dfrac{NV_{DC}-v_{uo}}{L_{leak}}\left(\dfrac{T_{sw}}{2}-\delta-\alpha\right) + i_2 \end{cases} \tag{3}$$

During the α interval, the matrix converter applies voltage to the u-w phase, and the inductor current flows from the u-phase side to the w-phase side.

In contrast, during the remaining intervals, the matrix converter applies voltage only to the u-phase, and the current flows from the u-phase to the neutral point o. Therefore, current flows continuously through the u-phase during T_{sw} / 2. Time-averaging the inductor current over these intervals gives the average u-phase current I_u, the neutral-line average current I_o flowing into the neutral point o, and the w-phase average current I_w. The average u–w-phase current I_{uw} is defined by (4) and given by (5).

$$I_{uw} = I_u - I_w \tag{4}$$

$$I_{uw} = \frac{2N\mathrm{V}_{dc}T_{sw}\delta - 4NV_{dc}\delta^2 + T_{sw}\alpha(v_{uo}-v_{uw}) - 2\alpha^2(v_{uo}-v_{uw})}{L_{leak}T_{sw}} \tag{5}$$

Similarly, the neutral-line average current I_o flowing into the neutral point o is obtained by time-averaging the current over the interval during which the matrix converter applies voltage only to the u-phase, as expressed by the following equation.

$$I_o = \frac{\alpha(T_{sw}-2\alpha)(NV_{dc}-v_{uw}) + 2NV_{dc}\delta(T_{sw}-2\delta) - 4NV_{dc}\alpha\delta}{2L_{leak}T_{sw}} \tag{6}$$

Equations (5) and (6) determine the time intervals δ and α within a switching period from the current command i_o^* and i_{uw}^*. The following discussion rearranges these equations with respect to α. For brevity, only the result for I_o is presented here. Equation (7) gives the resulting quadratic equation for α.

$$A_o\alpha^2 + B_o\alpha + C_o = 0 \tag{7}$$

Equation (8) gives the coefficients in (7). Applying the quadratic formula to (7) leads to the expression for α shown in (9).

$$\begin{cases} A_o = \dfrac{NV_{dc}-|v_{uw}|}{T_{sw}} \\ B_o = \dfrac{NV_{dc}-|v_{uw}|}{2} - \dfrac{2NV_{dc}\delta}{T_{sw}} \\ C_o = NV_{dc}\delta - \dfrac{2NV_{dc}\delta^2}{T_{sw}} - L_{leak}|I_o| \end{cases} \tag{8}$$

$$\alpha = \frac{-B_o \pm \sqrt{B_o^{\,2} - 4A_oC_o}}{2A_o} \tag{9}$$

Equation (9) includes the two unknowns α and δ. Therefore, the following analysis further rearranges the equation with respect to δ. As a result, (10) gives the quartic equation for δ, and (11) gives its coefficients.

$$a_4\delta^4 + a_3\delta^3 + a_2\delta^2 + a_1\delta + a_0 = 0 \tag{10}$$

$$\begin{cases} a_4 = 4NV_{dc}{}^4 - 8NV_{dc}{}^3v_{uw} + 4NV_{dc}{}^2v_{uo}{}^2 \\ a_3 = -4T_{sw}NV_{dc}{}^4 + 2T_{sw}NV_{dc}{}^3(v_{uo}+3v_{uw}) - 2T_{sw}NV_{dc}{}^2(v_{uo}{}^2 + v_{uo}v_{uw}) \\ a_2 = T_{sw}NV_{dc}[2L_{leak}\{I_o(NV_{dc}{}^2 - 2NV_{dc}v_{uo} + 2v_{uo}{}^2 - v_{uo}v_{uw}) \\ \quad + I_{dm}(NV_{dc}{}^2 - 2NV_{dc}v_{uw} + v_{uo}v_{uw})\} + T_{sw}NV_{dc}(NV_{dc}-v_{uo})(NV_{dc}-v_{uw})] \\ b = NV_{dc}(I_o + I_{dm}) + I_o(v_{uw}-2v_{uo}) - I_{dm}v_{uw} \\ a_1 = -\dfrac{1}{2}L_{laek}T_{sw}NV_{dc}{}^2(2NV_{dc} - v_{uo} - v_{uw})(b) \\ a_0 = \dfrac{1}{4}L_{leak}{}^2T_{sw}{}^2(b)^2 \end{cases} \tag{11}$$

Ferrari's method analytically solves the quartic equation in (10), giving up to four candidate solutions for δ. The analysis then selects a valid solution for δ. For each selected δ, (9) gives two candidate values of α. Physical constraints on δ and α therefore uniquely determine a feasible solution pair. The phase shift δ must be nonnegative because it determines the transmitted power in the high-frequency link. In addition, as in a DAB converter, a large δ increases the harmonic components of the transformer current and the reactive power. The analysis therefore limits δ to the range from 0 to T_{sw} / 4. The applied time α must also be nonnegative because it represents the interval during which voltage is applied across the u–w phase, as shown in Fig. 6. In this study, α is further

limited to T_{sw} / 2 or less in order to simplify the current model. The half switching period consists of the three intervals α, δ, and T_{sw} / 2 - δ - α. Therefore, all three intervals must remain positive, which requires $\delta + \alpha < T_{sw} / 2$. Moreover, the condition $\alpha > \delta$ is imposed because the current waveform model in Fig. 6 is derived only for this interval relationship. Accordingly, the analysis selects δ and α so that they satisfy all the conditions in (12).

$$0 < \delta < \frac{T_{sw}}{4}, \quad \delta \le \alpha < \frac{T_{sw}}{2} - \delta \tag{12}$$

This study assumes linear loads for basic verification. Future work includes extending the parameter-determination method to nonlinear loads and developing the analysis for current waveform modes other than that shown in Fig. 6.

IV. Simulation Results

A. Simulation Conditions

Table 1 shows the circuit parameters and control conditions used in the simulation. The study selected the system parameters on the basis of a Japanese single-phase three-wire residential distribution system. The u-w phase line-to-line voltage reference v_{uw}^* was set to 200 V_{RMS}, and the u-o phase voltage reference v_{uo}^* was set to 100 V_{RMS}. The output frequency was set to 50 Hz. The dc voltage V_{dc} was set to 400 V to represent a typical residential PCS battery voltage. The switching frequency f_{sw} was set to 50 kHz. The leakage inductance L_{lk} was set to 40 μH, and the output capacitors C_u and C_w were set to 4 μF each. To verify the control performance under unbalanced load conditions, the simulation used different load resistances for the two phases.

B. Simulation Waveforms

Fig. 7 shows the waveforms under an unbalanced-load condition without the proposed control. The upper traces represent the u–o-phase and w–o-phase output voltages, whereas the lower traces represent the phase currents, i_u, i_o, and i_w. Without neutral-line current control, each phase handles a different amount of active power, resulting in neutral-point potential fluctuation. Consequently, the u–o-phase and w–o-phase output voltages, which should have equal amplitudes and be 180 degrees out of phase under balanced-load conditions, become asymmetric and show an amplitude difference.

Fig. 8 shows the steady-state waveforms under the proposed control with unbalanced loads. The upper traces present the u–o-phase voltage, the w–o-phase voltage, the u-phase current, the w-phase current, the neutral-line current, the matrix-converter output voltage, the inverter output voltage, and the inductor current, whereas the lower traces show enlarged views of these waveforms. In Fig. 8, the simulation uses load resistances of R_u = 40 Ω and R_w = 10 Ω. The u–o-phase and w–o-phase voltages maintain almost the same amplitude even under unbalanced-load conditions. In addition, the neutral line carries the difference between the u-phase and w-phase currents, indicating compensation of the imbalance component. The enlarged lower traces also show that the control properly adjusts δ and α according to the load condition. The distortion near the zero crossing of the output voltage results from the limitation on the secondary-side duty ratio used to suppress the peak transformer current. Under this condition, the RMS voltage errors of v_{uo} and v_{wo}, relative to the reference value of 100 V_{RMS}, were within 1.1% and 1.5%, respectively. In addition, the THD of v_{uw}, calculated up to the 40th harmonic component, was 1.1%.

TABLE I. Simulation Conditions.

Symbol	Parameter	Value
v_{uw}^*	u-w phase line-to-line voltage	200 V_{RMS}
v_{uo}^*, v_{wo}^*	Phase voltage command	100 V_{RMS}
f_{out}	Output frequency	50 Hz
V_{dc}	DC voltage	400 V
f_{sw}	Switching frequency	50 kHz
$N_1 : N_2$	Turn ratio	1 : 1
L_{lk}	Leakage inductance	40 μH
C_u, C_w	Output capacitor	4 μF

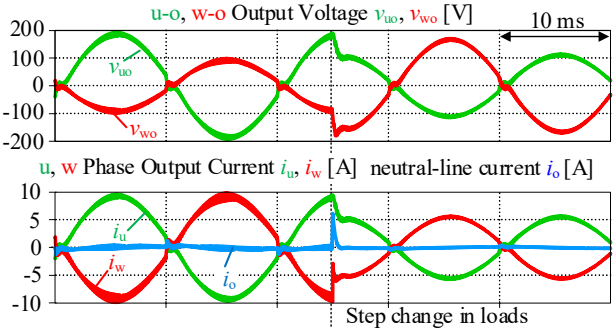

Fig. 7. Waveforms under an unbalanced-load condition without the proposed control.

These results confirm that the proposed control maintains constant output-voltage amplitudes by using the neutral-line current even under steady-state unbalanced-load conditions. Moreover, the enlarged traces confirm that the computed δ and α remain within the feasible region defined in (12), supporting the practical validity of the proposed parameter-determination method.

Fig. 9 shows the waveforms when the load condition is alternately switched between balanced and unbalanced states. The following discussion focuses on the transition interval from the balanced condition to the unbalanced condition. The output voltages v_{uo} and v_{wo} remain almost constant even when load imbalance occurs. Under the unbalanced condition, the neutral-line current appears, whereas almost no neutral-line current flows under the balanced condition. This result indicates that the neutral line carries the current imbalance caused by the unbalanced load, thereby allowing the converter to maintain the required phase voltages under unbalanced-load conditions.

Fig. 10 shows the waveforms during a load step. The following discussion focuses on the interval in which the power relationship between the u-phase and the w-phase reverses. The PI controllers keep the output voltages v_{uo} and v_{wo} almost constant even during the load step. Although the power relationship between the u-phase and the w-phase reverses during the transition, the converter stably supplies the required power in all cases.

V. Conclusion

This paper proposed a CVCF control method for a single-phase three-wire single-stage isolated AC-DC converter based on a single-phase matrix converter under standalone operation with unbalanced loads. The proposed method employs a line-

to-line voltage control loop and an imbalance compensation loop to suppress neutral-point potential fluctuation and maintain balanced phase voltages. In addition, this paper determines the control variables, δ and α, from the u-w phase current command i_{uw}^* and the neutral-line current command i_o^* based on an inductor-current waveform model. Furthermore, the proposed method selects the switching pattern according to the polarity relationship between the line-to-line voltage and the neutral-line current and thereby maintains stable CVCF operation even when the heavier-load phase changes. Simulation results demonstrated the effectiveness of the proposed method under steady-state unbalanced-load conditions, transitions between balanced and unbalanced loads, and load-step conditions. Experimental verification will be addressed in future work.

REFERENCES

[1] Reo Emoto, Shun Okamoto, Fuka Ikeda, Masayuki Okamoto, Hiroaki Yamada, and Toshihiko Tanaka, "ControlStrategy of Discharged Power with Bidirectional Battery Charger for EVs to Prevent Reverse Power Flow to UtilityGrid", IEEJ Journal of Industry Applications, Volume 13, Issue 3, pp. 346--347, 2024.

[2] Tsai-Fu Wu, Chh-Lung Shen, Chien-Hsuan Chang and Jeiyang Chiu, "1/spl phi/ 3W grid-connection PV power inverter with partial active power filter," in IEEE Transactions on Aerospace and Electronic Systems, vol. 39, no. 2, pp. 635-646, April 2003.

[3] Tsai-Fu Wu, Chih-Lung Shen, Hung-Shou Nein and Guang-Feng Li, "A 1/spl phi/3W inverter with grid connection and active power filtering based on nonlinear programming and fast-zero-phase detection algorithm," in IEEE Transactions on Power Electronics, vol. 20, no. 1, pp. 218-226, Jan. 2005.

[4] C. M. Liaw and S. J. Chiang, "Design and implementation of a single-phase three-wire transformerless battery energy storage system," in IEEE Transactions on Industrial Electronics, vol. 41, no. 5, pp. 540-549, Oct. 1994.

[5] C. Lung, H. Kakigano, Y. Miura and T. Ise, "Implementation of sigma-delta modulation controller for single-phase three-wire inverter in stand-alone operation applied for hybrid generation system for residential houses," 2013 IEEE 10th International Conference on Power Electronics and Drive Systems (PEDS), Kitakyushu, Japan, 2013, pp. 680-685.

[6] Yeong-Chau Kuo, Tsorng-Juu Liang and Jiann-Fuh Chen, "A high-efficiency single-phase three-wire photovoltaic energy conversion system," in IEEE Transactions on Industrial Electronics, vol. 50, no. 1, pp. 116-122, Feb. 2003.

[7] Shogo Nakahara, Satoshi Nagai, Makoto Ochiai, Yoshitaka Muguruma, Shinya Kawai, Hidemasa Yamaguchi, KenichiSaruta, and Hidetoshi Kanazawa, "Development of Dual Active Bridge DC-DC Converter to Achieve High Efficiency inWide Voltage and Load Range and Application to V2H Systems", IEEJ Journal of Industry Applications, Volume 13,Issue 4, pp. 475--488, 2024.

[8] Kazuma Tomida, Kenji Natori, Jin Xu, Noboru Shimosato, and Yukihiko Sato, "A Novel Control Method to ImproveEfficiency in Wide Output Voltage Range for Bidirectional Isolated Three-Phase AC/DC Converter Based on MatrixConverter", IEEJ Journal of Industry Applications, Volume 13, Issue 1, pp. 17--23, 2024.

[9] B. P. Do, M. Gerado Geda, H. -P. Kieu and S. Choi, "A Half-Bridge Single-Stage AC–DC Converter With Single- and Three-Phase Compatibility," in IEEE Journal of Emerging and Selected Topics in Power Electronics, vol. 13, no. 6, pp. 8051-8061, Dec. 2025.

[10] H. Kim, J. Park, S. Kim, R. M. Hakim, H. Belkamel and S. Choi, "A Single-Stage Electrolytic Capacitor-Less EV Charger With Single- and Three-Phase Compatibility," in IEEE Transactions on Power Electronics, vol. 37, no. 6, pp. 6780-6791, June 2022.

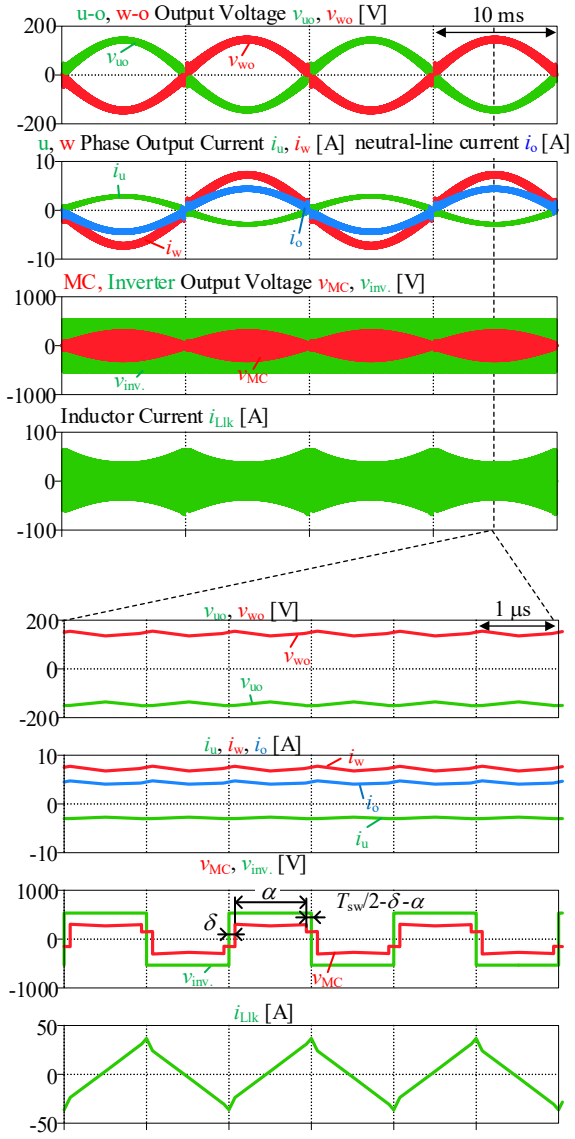

Fig. 8. Operation waveform of steady state in unbalance loads condition.

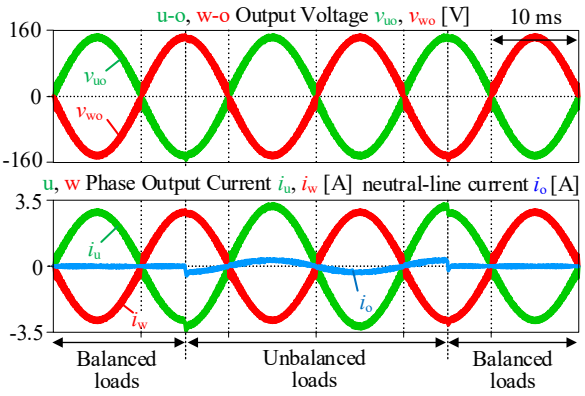

Fig. 9. Operating waveforms during transitions between balanced and unbalanced loads conditions.

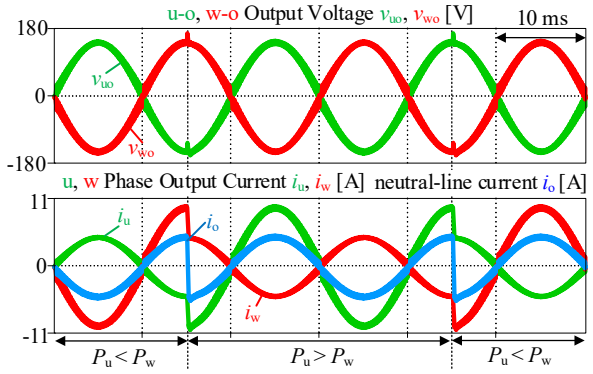

Fig. 10. Operating waveform during a loads step.